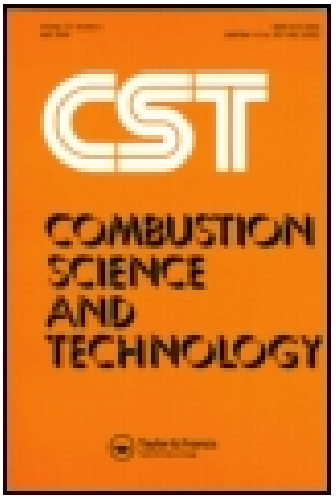

Combustion Science and Technology
Publication details, including instructions for authors and subscription information:
http://www.tandfonline.com/loi/gcst20

Modeling of Spherically Symmetric Droplet Flames Including Complex Chemistry: Effect of Water Addition on n-Heptane Droplet Combustion

G. S. JACKSON [a] & C. T. AVEDISIAN [a]
[a] Sibley School Of Mechanical , and Aerospace Engineering Cornell University Ithaca , New York, 14853-7501
Published online: 05 Apr 2007.

Combust. Sci. Tech., 1996, Vol. 115, pp. 125–149
Reprints available directly from the publisher
Photocopying permitted by license only

Modeling of Spherically Symmetric Droplet Flames Including Complex Chemistry: Effect of Water Addition on n-Heptane Droplet Combustion

G. S. JACKSON[1] and C. T. AVEDISIAN[2]

Sibley School Of Mechanical and Aerospace Engineering Cornell University Ithaca, New York 14853-7501

(Received 7 July 1995; in final form 22 February 1996)

A spherically symmetric quasi-steady model has been formulated for droplet combustion which includes complex chemistry and variable properties. The model is applied to mixtures of heptane and water.

Calculations from the model show that the acetylene concentration inside a heptane flame increases with increasing droplet diameter. This trend suggests an increased propensity for soot formation with increasing droplet diameter which is in agreement with some qualitative trends from experiment. Predicted quasi-steady burning rate constants for pure heptane droplets, however, do not vary with droplet diameter which may be attributed to the model's inability to account for the physical presence of soot particles and aggregates and their effect on heat transfer to the droplet. The addition of water to heptane is found to lower burning rates and C_2H_2 concentrations, and a limiting water concentration for stable burning is predicted, similar to prior reported analyses based on a simplified one-step reaction mechanism.

Keywords: Droplet combustion; emulsions; complex chemistry; water addition; soot

NOMENCLATURE

c_{pi} specific heat capacity of species i in gas phase
D_i mass diffusivity of species i in the gas phase
D_{T_i} Soret diffusion coefficient of species i in the gas phase

[1]Current address: Precision combustion, INC., 25 Science Park, New Haven, ct. 06511-1968.
[2]author to whom correspondence should be addressed.

h_i enthalpy per unit mass of species i
K droplet burning rate constant
L_i heat of vaporization per unit mass of species i
$\dot{m}$ mass flow rate
R universal gas constant
r radial position from center of droplet
r_d droplet radius
r_p effective radius of soot agglomerate
r_{sh} radial location of soot shell structure
T gas phase temperature
T_d droplet temperature
V_i diffusion velocity of species i in the gas phase
v_g gas phase radial velocity
x gas phase mole fraction of air
Y_i mass fraction of species i in gas
Y_{il} mass fraction of species i in liquid

Greek symbols

ε_i mass fractional vaporization of ith species
λ thermal conductivity of gas phase mixture
ρ gas phase density
ρ_l liquid phase density
ω_i net mass production rate of species i per unit volume

1. INTRODUCTION

Theoretical models of spherically symmetric droplet combustion assume symmetric ignition, no relative droplet/gas velocity and hence no internal circulation, and negligible buoyancy. Under these conditions, the flow field in the surrounding gas is one-dimensional, and the flame is spherical and concentric with the droplet as depicted in Figure 1. When soot forms under these transport conditions, the particles can become trapped between the droplet and its flame due to a balance of the drag and thermophoretic forces on the particles. The presence of these microscopic soot particles and their subsequent growth into large aggregates inside the droplet flame can influence the droplet burning process. For example, the formation of soot can reduce the chemical heat release rate and as a result, the droplet vaporization rate from the ideal case when all fuel molecules are transported to the flame and oxidized.

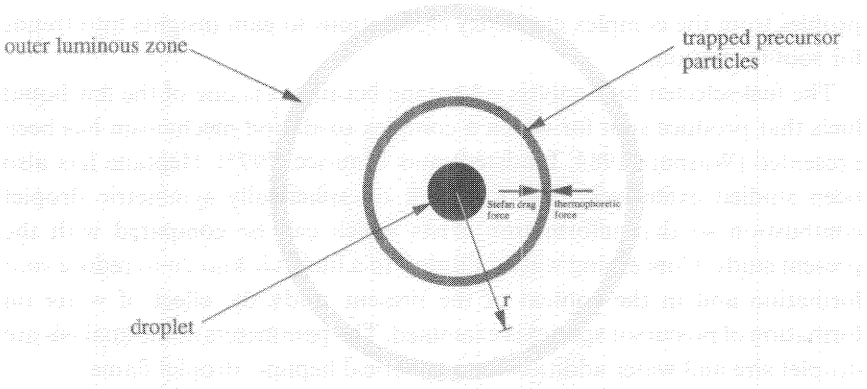

FIGURE 1 Schematic of idealized spherically symmetric configuration.

An extensive literature on soot formation in flames exists (e.g., Haynes and Wagner, 1981; Glassman, 1988). However, relatively little work has been reported which specifically models soot formation in the context of droplet combustion. The uncertainties in the soot formation process as well as the characterization of soot particle transport present difficulties in formulating a droplet combustion model which accounts for soot formation. Necessary ingredients to a comprehensive model of soot formation in spherical droplet flames should include 1) complex chemistry, 2) formation of soot precursor species, 3) surface growth and agglomeration of particles, 4) entrapment of aggregates to form the soot shell, and 5) such aspects of the transport process as gas phase unsteadiness, variable physical properties, and radiation. Submodels for some of these aspects have been presented (e.g., Kesten *et al.*, 1980; Cho *et al.*, 1992; Jackson *et al.*, 1992; Saitoh *et al.*, 1993;).

Increased computational power and the availability of 'complex' oxidation mechanisms for several fuels now make it possible to incorporate complex chemistry in modeling droplet combustion processes which can provide more realistic predictions of the flame dimensions and the concentrations of minor species associated with soot precursor formation. The present study incorporates such a complex chemical mechanism in order to provide some insights on how formation of soot precursor species is influenced by the initial droplet diameter and water mixed with the fuel. The purpose was to isolate the influence of complex chemistry on the spherically symmetric droplet burning problem to 1) compare the results with published models for droplet burning in which single step reactions were assumed, and 2) use computed species

profiles from the complex chemistry calculations to gain insights into trends for soot formation.

The fuel selected for analysis is heptane because it is one of the few liquid fuels that produce soot for which a complex oxidation mechanism has been presented (Warnatz 1984; Lindstedt and Maurice, 1995). Heptane has also been studied extensively in prior work on spherically symmetric droplet combustion so that information exists which can be compared with the present study. Concerning water addition to a fuel, it is known to reduce soot formation and in the context of the present study the effect of water on formation of precursor species is examined. The parameters in the analysis are droplet size and water addition for a spherical heptane droplet flame.

Soot particle formation is not specifically included and, therefore, the results approximate conditions for which soot formation would not be significant enough to influence the overall droplet burning process. Experiments suggest that this situation is approached when the initial droplet diameter, oxygen concentration, and/or pressure are reduced (Jackson and Avedisian, 1994; Choi *et al.*, 1990). In this 'soot-free' limit (of an otherwise sooting fuel) the extent to which the gasification rate and concentration of soot precursor species depends on droplet diameter and water mixed with the fuel is analyzed when complex chemistry and variable properties are included in the analysis.

The present study builds on prior work in which a one-step reaction mechanism and quasi-steady conditions were assumed in modeling heptane droplet combustion. Although the quasi-steady assumption is being made, experiments (Okajima and Kumagai 1975; Jackson and Avedisian 1994) show a time varying ratio of luminous zone (flame) to droplet diameter for near spherically symmetric burning conditions in contrast to quasi-steady conditions for which this ratio is independent of time. Results from the present study would likely be most applicable to this asymptotic period of burning, as well as to the steady flames produced around porous spheres fed with a constant fuel flow rate.

Puri and Libby (1991) employed a single-step flame sheet reaction and variable gas-phase properties to analyze heptane droplet combustion. A similar model was presented for combustion of a heptane/water emulsion droplet (Law, 1977) but further assumed constant gas phase properties. Some results from these two studies are compared with the present one. Card and Williams (1991) coupled a reduced kinetic mechanism with the quasi-steady assumption for heptane, but assumed constant properties. Concerning time-dependent models, complex kinetic mechanisms were incorporated in a model of combustion of a non-sooting methanol droplet (Cho *et al.*, 1990, 1992).

Because complex chemistry is included in the current model, the distribution of various species which are considered to be the primary small hydrocarbon species contributing to soot formation can be calculated. Acetylene is used as the primary precursor for soot in this regard (Haynes and Wagner, 1981; Glassman, 1988). By using an approximate expression for the soot nucleation rate (Fairweather *et al.*, 1992) which is proportional to acetylene concentration, the mass fraction of vaporized fuel which is converted to soot can be determined.

2. ASSUMPTIONS

The following assumptions are made for the one-dimensional droplet flame model:

1) steady-state gas and liquid phase temperatures and compositions;
2) no spatial variation in the liquid phase composition or temperature;
3) ideal gas law;
4) Fick's law of diffusion;
5) no particulates in gas phase;
6) negligible radiative heat transfer.

Consistent with these assumptions, the conservation equations for a radially symmetric flow field (Fig. 1) can be written as

$$\dot{m} = 4\pi\rho r^2 v_g = \text{constant} \tag{1}$$

for mass conservation,

$$\dot{m}\frac{dY_i}{dr} + \frac{d}{dr}(r^2\rho Y_i V_i) - r^2\omega_i = 0 \tag{2}$$

for conservation of the "ith" species (23 in all with 96 reactions for the mechanism considered (Warnatz 1984)), and

$$\dot{m}\sum_{i=1}^{n}(Y_i c_{pi})\frac{dT}{dr} - \frac{d}{dr}\left(r^2\lambda\frac{dT}{dr}\right) + \rho r^2\sum_{i=1}^{n}(Y_i V_i c_{pi})\frac{dT}{dr} + r^2\sum_{i=1}^{n}h_i\omega_i = 0 \tag{3a}$$

for overall energy conservation where $n = 23$. The enthalpy, h_i, in eq. 3a is

$$h_i = h_i^0 + \int_{T_0}^{T} c_{pi} dT \tag{3b}$$

where T_0 is a reference temperature which by convention is 0 °K and the c_{pi} are assumed to be temperature dependent. The mass weighted diffusion velocity of the ith species, $Y_i V_i$, can be written as

$$Y_i V_i = -D_i \frac{dY_i}{dr} + \frac{D_{Ti}}{T} \frac{dT}{dr} \tag{4}$$

To insure mass balance, calculated mass-weighted diffusion velocities ($Y_i V_i$) are corrected by a uniform velocity in order that $\sum_{i=1}^{n} Y_i V_i = 0$.

For boundary conditions at the droplet surface, the droplet temperature (T_d) and gas phase species concentrations are determined by vapor-liquid equilibrium. Droplet temperatures for both the pure heptane and heptane/water mixture droplets are expected to be slightly lower than the heptane boiling point for equilibrium vaporization conditions since heptane has a normal saturation temperature 1 °K lower than that of water. The inability for vapor equilibrium to be maintained for both phases of an emulsion (Wang, 1984) suggests that the droplet temperature for the heptane/water droplet is probably closer to the heptane boiling point than the actual equilibrium vaporization temperature which is lower.

The simplest assumption to make about the temperature of a burning droplet is that it is at the boiling point of the fuel. The uncertainty with this assumption was assessed semiquantitatively by imposing T_d values ranging from the boiling point of heptane to as low as 350 °K. Results of these calculations (not reported here) were found to be relatively insensitive to changes of T_d in this range. Over this range, the calculated droplet burning rate decreased by less than 2%, the flame radius (based on maximum temperature) decreased by less than 5%, and the maximum flame temperature fell by approximately 5 °K. These comparatively small changes for the conditions considered here show that, consistent with a suggestion from prior analyses (Williams, 1985), it is reasonable to assume a fixed temperature for the droplet surface as the boiling point of the fuel (372 °K for heptane).

Another issue involves the potential for heat conduction into the liquid phase due to a spatially nonuniform droplet temperature. This question also arises because of the boundary condition at the droplet surface. For the

conditions examined here, calculations were carried out by arbitrarily imposing a surface temperature gradient at the droplet surface (in the liquid phase) as high at $2^*(T_d - T_\infty)/r_d$. The results showed that the burning rate did not change by more than 3% from the uniform droplet temperature case.

With the above assumptions, boundary conditions for the problem are as follows.

At $r = r_d$:

$$r^2 \rho Y_i V_i - \dot{m}(\varepsilon_i - Y_i) = 0 \tag{5}$$

$$\dot{m} \sum_{i=1}^{n} \varepsilon_i L_i - r^2 \lambda \frac{dT}{dr} = 0 \tag{6}$$

$$T = T_d \tag{7}$$

At $r = \infty$:

$$Y_i = Y_{i\infty} \tag{8}$$

$$T = T_\infty \tag{9}$$

where the far ambience is room temperature air at atmospheric pressure for the current study. Because internal circulation does not occur when spherical symmetry is assumed, and the emulsion components are assumed to be immiscible, only that amount of dispersed phase which is exposed at the droplet surface by the receding liquid/vapor interface is vaporized. The droplet composition is constant throughout combustion under these conditions for a single component continuous phase and $\varepsilon_i = Y_{il}$. The constant composition approximation corresponds to a so-called 'frozen limit' which can only be applied (Law 1977) to quasi-steady periods during emulsion droplet burning. Unsteady phenomena associated with preferential vaporization cannot be taken into account with such a model.

D_i, D_{Ti}, and λ, are evaluated with a previously tested model (Coffee and Heimerl, 1981; Kee *et al.*, 1986), while c_{pi} and h_i are found from the CHEMKIN thermochemical data base (Coffee and Heimerl, 1981). Liquid property values are taken from Vargaftik (1975). Reaction rates are calculated from user-provided rate parameters, and thermochemical data are processed by the CHEMKIN interpreter (Kee *et al.*, 1987).

The choice of the kinetic mechanism for heptane was based on anticipated computational time and accuracy. The mechanism proposed by Warnatz (1984) consists of 96 steps and 23 species. A more extensive kinetic mechanism for heptane recently proposed by Lindstedt and Maurice (1995) consists of 659 elementary reactions and 109 species. In this phase of our modelling, we selected the Warnatz (1984) scheme in the context of the spherical heptane droplet flame because of its fewer number of reaction steps and the anticipated reduction in computational time relative to the much larger scheme. Furthermore, it has been used with some success in modeling the related heptane counterfow diffusion flame. (Bui-Pham and Seshadri, 1991). Since the goal of the present study was to illustrate trends when detailed chemistry is incorporated into a droplet combustion model for a sooting fuel, any reasonable kinetic mechanism could be used for that purpose. The particular numerical algorithm which we used to solve the conservation equations, however, (described in Section 3) is capable of incorporating any kinetic mechanism.

The Warnatz (1984) scheme does not take into account the wide range of possibilities for the splitting of the C_7H_{15} radical (Westbrook, 1986) and over-predicts the amount of C_3H_6 formed. However, the breakdown of larger hydrocarbons into C_2 and C_1 species occurs well before the flame front. Thus, the high C_3H_6 production does not significantly change the oxidation at the flame front.

3. NUMERICAL ALGORITHM

A numerical algorithm similar to the one employed for analyzing counterflow diffusion flames (Smooke, 1991) is used to solve discretized versions of the governing differential equations for the spherically symmetric steady droplet flame. This algorithm uses time integration of the corresponding unsteady problem to provide a guess for Newton's method to find the final solution for the steady state discretized temperature and species profiles.

The present model uses a finite differencing scheme to solve the governing equations. Details are given elsewhere (Jackson, 1994). After discretization, the problem becomes one of solving a set of non-linear coupled algebraic equations, where the solution vector consists of $Y_{i,j}$ and T_j at each node j in the computational mesh between the droplet surface r_d and the radius at "infinity", r_∞(theoretically, $r_\infty = \infty$).

For the numerical solution, the outermost nodal point situated at r_∞ must have a finite value. If it is too large, computational time can be excessive and if

it is too small the numerical solution will not be accurate. A value for r_∞ was selected by determining a value below which the transient droplet combustion process would influence the oxygen species concentration during the droplet lifetime. From such calculations, it was determined that the region of influence of the transient droplet combustion process was approximately $100\,r_d$. The droplet vaporization rate was found to be insensitive to changes in r_∞ above $100\,r_d$, and this value was used for the solutions presented in this study.

An initial guess for the numerical algorithm is based upon an analytical solution from classical quasi-steady droplet combustion theory (Glassman, 1987) for the major species, which are the vaporizing fuel species, O_2, H_2O, CO_2, and N_2. All other species are given Gaussian profiles with peaks either at the initially guessed flame location or inside the flame depending on the expected peak locations in the diffusion flame. The location of the flame for the initial guess is specified by the user rather than calculated from fuel properties. The time-stepping algorithm pushes this initial guess closer to the final solution before Newton's method is initiated.

Once a steady state solution is found for a particular mesh, the mesh is refined until no more mesh refinement is necessary by a previously described refinement criterion (Smooke, 1991). In general, for the flames modeled in this study the final converged solution has between 150 and 300 mesh points. Computations were done on a Silicon Graphics Indigo Workstation (with an R8000 microprocessor). Typical computational times ranged from 2 hrs to 4 hrs depending on the difficulty of convergence.

4. HEPTANE

4.1. Species Profiles

Numerical results are reported for droplet radii, r_d, ranging from 0.08 mm to 0.50 mm. When the droplet radius was decreased below 0.08 mm, the final solution showed extinction of the chemical reactions which suggests that 0.08 mm may approximate an extinction radius for heptane for the reaction scheme considered. This value is within the range of predictions by Card and Williams (1991) for the reduced reaction scheme they considered in their constant property analysis of heptane droplet combustion (cf, Fig. 8 in Card and Williams, 1991). However, in an actual droplet combustion experiment, the flame is not steady but moves in toward the droplet to sustain combustion before undergoing extinction, and these effects are not considered in the analyses.

Figure 2 illustrates the variation of some important gas phase species with r_d for a pure heptane droplet flame. The increased time for pyrolysis in the larger droplet flames results in the destruction of C_7H_{16} occurring at lower values of r/r_d as r_d increased as shown in Figure 2. This increased time for pyrolysis causes an increase in the formation of intermediates such as C_2H_2: the mass fraction profile of C_2H_2 for the 0.50 mm radius heptane droplet peaks at a value five times higher than for the profile of the 0.10 mm heptane droplet. Figure 2 also shows that as r_d increases, proportionately less O_2 diffuses through the oxidation zone unreacted, and proportionally less CO is transported out of the flame toward the ambience. This result suggests that more complete oxidation occurs as the droplet size increases. The increase in O_2 leakage is not significant enough to alter the droplet burning rate constants as discussed in the next section.

Figure 3 compares predicted heptane and oxygen species distributions with results reported by Puri and Libby (1991). The effect of the flame sheet approximation is evident as the species distributions are essentially zero at the 'flame front' in the calculations reported by Puri and Libby (1991), which from the results shown in Figure 3 is at $r/r_d \approx 10$. On the other hand, the results in Figure 2 show a continuous distribution of oxygen throughout the gas phase. The complex kinetic scheme considered here suggests a much broader reaction zone where C_7H_{16} and O_2 mass fractions are below 10^{-3} and reactive intermediates have relatively high concentrations.

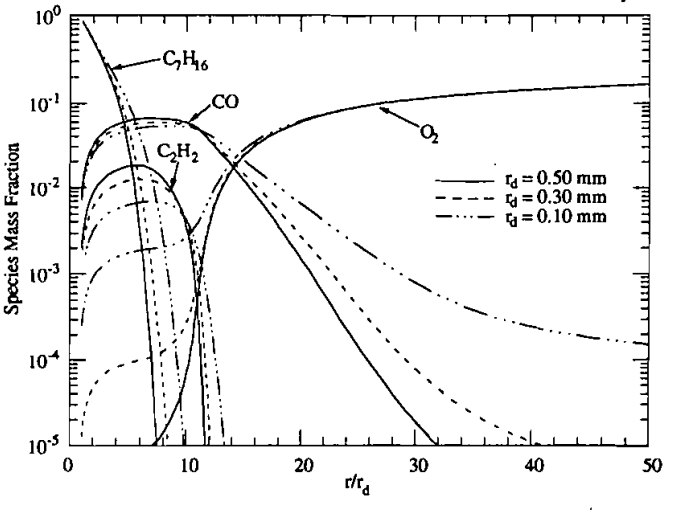

FIGURE 2 Distribution of various species around heptane droplets of several different radii.

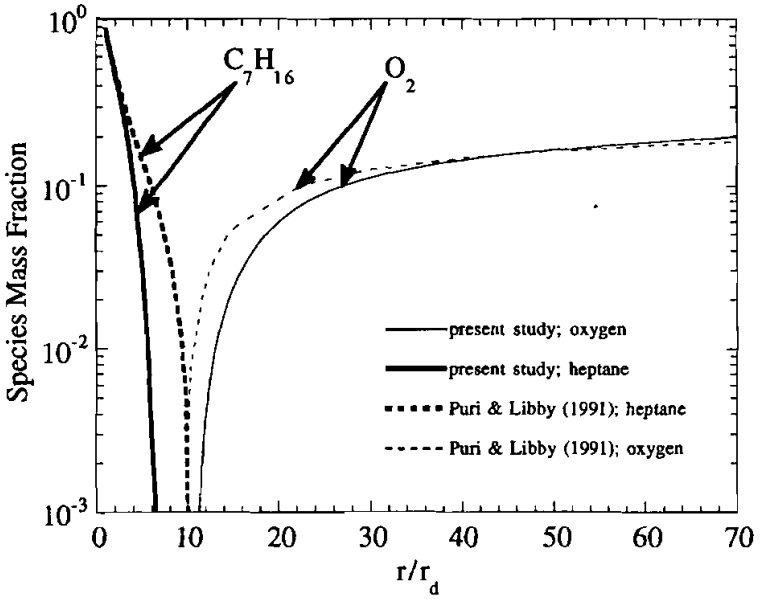

FIGURE 3 Comparision of results with model of Puri and Libby (1991).

4.2. Temperature Profiles and Burning Rate Constants

The flame front can be defined in various ways, such as by the peak in OH mass fraction or by the peak temperature. The temperature profiles in Figure 4 for different heptane droplet flames consistently peak at $r/r_d \approx 11$ and the OH profiles reach their maximums at $14 < r/r_d < 15$. Both OH and temperature peaks indicate flame zones further out than measured flame locations (between $6r_d$ and $8r_d$) from microgravity droplet combustion experiments (Jackson and Avedisian, 1994). Several reasons for the disparities are the following: the flame never reaches its quasi-steady location for the droplet sizes investigated in the experiments; the luminous boundary may not correspond to the location of peak temperature in the droplet combustion experiments; or the model does not incorporate the influence of soot formation.

The temperature profiles for various sized droplets are coincident near the droplet surface as shown in Figure 4. Using the relationship $\dot{m} = K\rho_1 r_d/8$, coincident temperature profiles near the droplet surface for different droplet

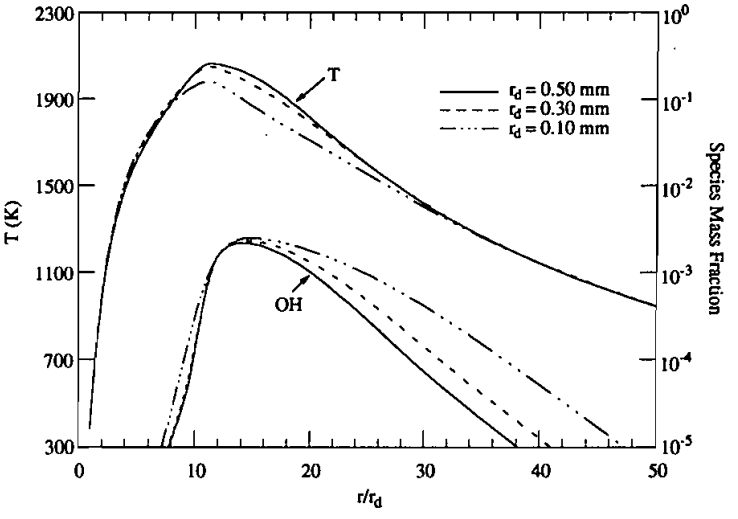

FIGURE 4 Variation of gas phase temperature and OH species with radial location for droplets of different radius, r_d.

sizes imply similar burning rate values since K can be expressed as

$$K = \frac{8\lambda}{\rho_1 \sum_{i=1}^{m} \varepsilon_i L_i} \frac{dT}{d(r/r_d)} \tag{10}$$

where the gradient is evaluated at $r = r_d$. Actually, K was found to vary over a small range, 0.86 to 0.87 mm^2/s, for the range of droplet sizes considered.

Figure 5 compares the temperature distribution reported by Puri and Libby (1991) with the calculations of this study for the 0.5 mm radius droplet of Figure 4, (results for smaller radii yielded larger differences). The effect of the flame sheet approximation is evidenced by the sharp peak in temperature at $r/r_d \approx 10$ for the previous results (Puri and Libby, 1991). By contrast, the temperature distribution calculated here shows a broader and lower peak due to the exothermic oxidation reactions occurring over a distributed reactive zone. However, the location of the peak temperature, which is often used to define the position of the flame, is nearly the same for the two calculations. The agreement in flame locations of the two models suggests that the differences in reaction kinetics do not overwhelm the similarity in fuel transport to the flame zone.

The present analysis does not account for soot particle formation and the conversion of fuel molecules to soot. A nonzero soot formation rate should

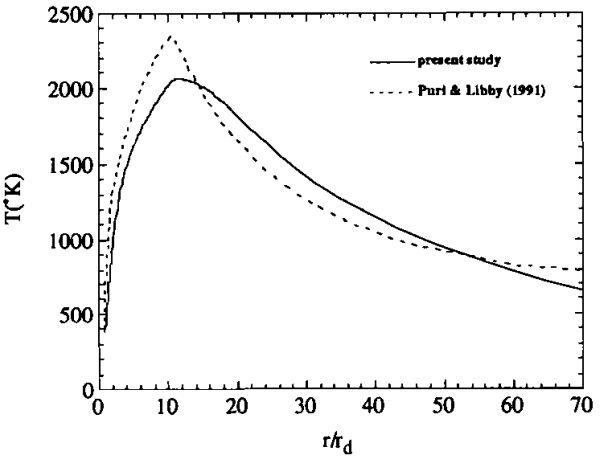

FIGURE 5 Variation of gas phase temperature with radial position for a .5 mm radius heptane droplet.

lower both the heat release at the flame and the gasification rate compared to the situation considered here in which essentially no conversion of fuel to soot particles is accounted for. As the droplet size increases, some limited information exists (e.g., Jackson *et al.*, 1992; Jackson and Avedisian, 1994; Gupta *et al.*, 1994) which shows that the amount of soot formed increases, both absolutely and when proportioned to the mass of fuel burned. Based on this, the gasification rate predicted by the present model would be an upper bound for heptane which is approached by very small droplets which burn with virtually no soot formation-a kind of 'soot-free' burning rate limit for a sooting fuel. Such a limit might also be reached for larger droplets if experimental conditions effect fuel molecule transport to the flame, such as convection which can also break up the delicate soot shell and alter its shape.

The predicted value of about 0.86 mm^2/s, essentially independent of droplet size, is about 15% higher than droplets with d_0 about 0.5 mm (Jackson and Avedisian, 1994), and 50% higher than measured for 1.0 mm diameter droplets (Choi *et al.*, 1990; Jackson and Avedisian, 1994). The 15% difference for smaller droplets where soot formation may not be significant is likely due to a combination of uncertainties in property value correlations (with temperature and composition) used in the model, and experimental uncertainty. For the 1.0 mm diameter droplets, differences with experiment are substantial and outside the range of uncertainty in either the model results or experimental data. However, several investigators have also reported gasification rates for

large (1.0 mm) droplets which are quite close to the small (0.5 mm) droplet values, and it has been speculated (Choi *et al.*, 1990) that factors may have been present in the experiment that promoted soot particle and fuel molecule transport to the flame. For example, the limiting value of K predicted here is consistent with some prior reported gasification rate values for heptane droplets with initial diameters of about 1.0 mm (e.g., Chauveau *et al.*, 1993; Okajima and Kumagai, 1975) in which spherical soot shells were not specifically observed, because of the reasons cited above. Evidently, it is difficult to create the requisite degree of sphericity in all stages (ignition to burnout) of a droplet burning experiment to obtain gasification rates for 'large' droplets ($d_0 \gtrsim 1$ mm) that would be significantly lower than K for 'small' droplets ($d_0 < 0.5$ mm).

4.3. Soot Shell Predictions and Propensity for Soot Formation

Soot formation is neglected in this model due in part to the difficulty of accurately modeling particle movement and aggregate growth inside the flame. However, temperature gradients and Stefan velocities can certainly be calculated from the numerical solutions. A fictitious situation is considered in which a particle resides between the droplet and flame but does not influence the transport processes. Forces acting on the particle are calculated to find the location where they balance. Equations from Jackson *et al.*, (1992) are used to calculate the inwardly directed thermophoretic force and the outwardly directed drag force due to Stefan flow, with the thermophoretic force being based on the formulation of Talbot *et al.*, (1980). The particles are assumed to be spherical because formulations for nonspherical particles are not yet available.

Predicted radii, r_{sh}, where forces balance on soot particles of radius r_p are shown in Figure 6. Particles with r_p less than 10.0 μm are predicted to reside at a radial location midway between the droplet surface and the flame boundary. The soot shell position is relatively insensitive to particle radius for $r_p < 1$ μm and particles less than about 1 μm will be trapped in a narrow location, $\xi_{sh}(\equiv (r_{sh} - r_d)/(\dot{r}_f - r_d))$, of just less than 0.6 as shown in Figure 6. As r_p increases above 1 μm, ξ_{sh} rapidly increases, and for $r_p > 5$ μm no particles are trapped inside the flame. The predicted location where forces balance shown in Figure 6 is larger than observed in some experiments (r_{sh}/r_d around 3 (Jackson and Avedisian 1994)). The difference may be due in part to the fact that the model assumes a quasi-steady flame and predicts larger flame diameters than measured. Larger flames decrease temperature gradients which result in lower thermophoretic forces.

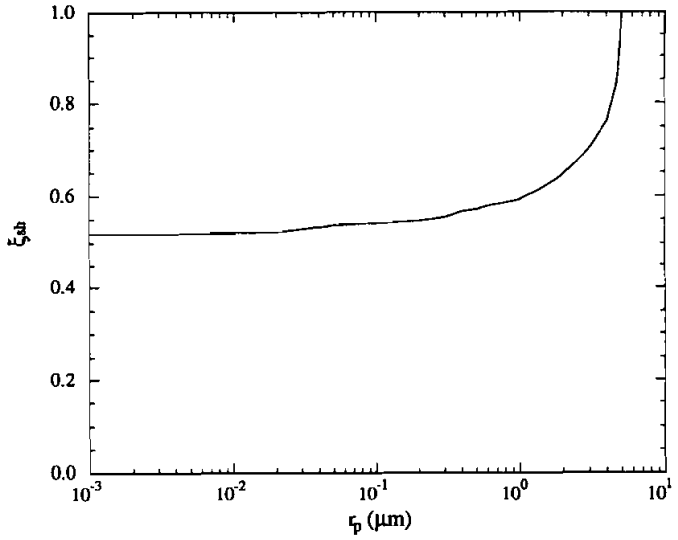

FIGURE 6 Non-dimensional radius, ξ_{sh}, where forces balance on particles of radius r_p.

The stability of the soot shell is determined by the gradient of the net force acting on soot particles. Figure 7 shows the variation of net force ζ (non-dimensionalized by a calculated Millikan drag force) for three values of r_p. Two positions where forces on particles balance (corresponding to $\zeta = 0$) are indicated: one near the droplet (#1) and another closer to the flame (#2). The stable position corresponds to $d\zeta/d\xi|_{\xi=\xi sh} < 0$, or position #1 in Figure 7, while the entrapment position closer to the flame (#2) is unstable. Flow perturbations at position #2 will either push particles inward to position #1 or move them out through the flame beyond which both thermophoretic and drag forces act in the direction away from the droplet (at the flame front ($\zeta = 1$), $\partial T/\partial r = 0$ and the thermophoretic force is zero).

For the stable shell position shown in the blown-up region in Figure 7, $d\zeta/d\xi$ decreases as r_p increases (see inset). This means that smaller particles are more likely to be locked into the shell than larger particles. As aggregates continue to grow they become more vulnerable to gas phase disturbances from convective flows because of the reduced magnitudes of thermophoretic and Stefan drag forces acting on them. Break-up of the shell is thus more likely to be initiated by larger aggregates which form later in the burning history and drift outward. This trend is in qualitative agreement with experimental observa-

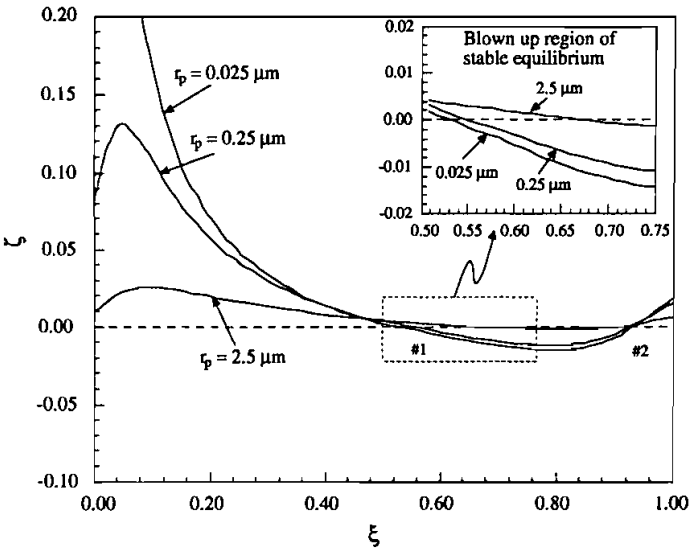

FIGURE 7 Distribution of net force on particles of radius r_p around a burning heptane droplet.

tions that have shown such outward drifting of large aggregates (Jackson and Avedisian, 1994).

Figure 2 previously showed the distribution of C_2H_2 around droplets for three droplet radii. Generally, higher peak concentrations are realized as r_p increases, but the concentration also broadens as r_p decreases. To better quantify C_2H_2 formation which we assume to be a primary precursor to soot, the total amount of C_2H_2 formed between the droplet and flame is calculated by integrating the C_2H_2 distribution:

$$\dot{m}_{soot} = \int_{r_d}^{r_\infty} \left(r^2 \rho Y_{C_2H_2} W_{soot} A \exp\left[\frac{-E_a}{RT}\right] \right) dr \tag{11}$$

where $r_\infty \approx 100 r_d$ as discussed in Section 3. Dividing $\dot{m}_{soot}$ by the mass evaporation rate of fuel, $\dot{m}_{fuel}$, gives the proportional amount of soot formed per unit mass of fuel vaporized. An increased tendency for vaporized fuel to produce soot would imply a decrease in the heat release at the flame due to fewer fuel molecules oxidizing at the flame and hence lower heat transfer to the droplet. A variation of K with r_d should then track with the variation of $\dot{m}_{soot}/\dot{m}_{fuel}$ with r_d.

Parameters in eq. 11 were taken from Fairweather *et al.*, (1992). The pre-exponential A is $10.36*10^6\,s^{-1}$, the activation energy E_a is set at 172 kJ/mole and W_{soot} is 12000 g/mol. The variation of $\dot{m}_{soot}/\dot{m}_{fuel}$ with r_d is shown in Figure 8 for heptane droplets in the range $0.08 < r_d < 0.5$ mm. As r_d increases, the fraction of vaporized fuel which should go to soot formation increases (from 0.2% for $r_d = 0.1$ mm to 6.6% for $r_d = 0.5$ mm). By inference, the chemical energy released at the flame would be reduced accordingly which in turn will reduce the heat flux to the droplet and lower the gasification rate. Thus, although the model does not directly account for soot formation and therefore predicts burning rates for heptane droples which do not vary substantially with r_d, it does suggest that soot formation would increase with r_d. This general trend has been qualitatively observed in microgravity experiments (Jackson and Avedisian, 1994), and more quantitatively for droplets burning in a convective environment (Gupta *et al.*, 1994).

5. HEPTANE/WATER MIXTURES

5.1. Species Profiles and Propensity for Soot Formation

Figure 9 shows the distribution of several gas phase species around steady droplet flames (with $r_d = 0.30$ mm) of heptane/water emulsions with the indicated initial water content as the parameter. As the water concentration

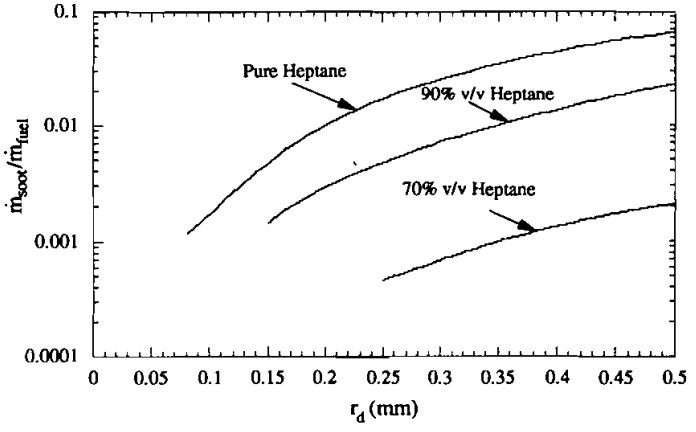

FIGURE 8 Effect of droplet radius on propensity for soot formation for various heptane/water mixtures.

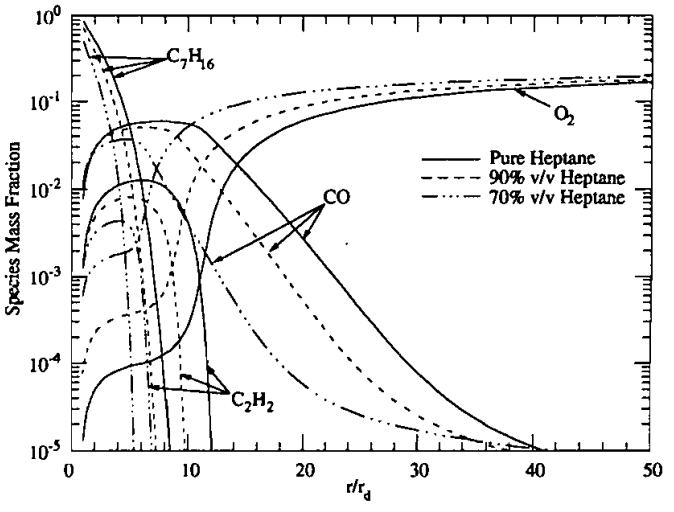

FIGURE 9 Distribution of various species around a heptane/water emulsion droplet.

inside the droplet increases, the profiles for O_2 move in toward the droplet surface which indicates a decrease in flame diameters. More O_2 leaks through the flame zone as the water content increases, which may be partly caused by thinner flames. Figure 9 also shows that peaks in CO and C_2H_2 mass fraction profiles decrease with increasing liquid water content. The reduction in CO may be caused by the increased H_2O inside the flame pushing the water-gas shift equilibrium toward CO_2. Decreases in C_2H_2 mass fractions may result in part from decreased time for fuel pyrolysis due to smaller flames as the water content increases.

The propensity for soot formation in heptane/water mixture flames is approximated in the same manner as for pure heptane droplet flames. $\dot{m}_{soot}$ is evaluated from Equation 11 for 70% and 90% by volume heptane/water emulsions. Results are shown in Figure 8 where $\dot{m}_{fuel}$ for the heptane/water mixtures includes only the mass of heptane vaporized. The decrease in the fraction of heptane going to soot formation shows the effectiveness of the vaporizing water in reducing the propensity for soot formation. Small increases in liquid water content substantially decrease the propensity for soot formation for a given amount of fuel burned. The model results suggest that a 10% by volume water addition reduces the propensity for soot formation by approximately 4 times for a given droplet size, and further that 30% by volume water addition decreases the soot formation by as much as 40 times. The

reduction in soot formation with increasing water content may be explained by the effect of water on reducing the flame diameter along with the associated time for fuel pyrolysis and on causing a more rapid rise in the concentration of oxidizing OH radicals.

5.2. Temperature Profiles and Burning Rate Constants

Figure 10 shows the distribution of OH and temperature in the gas surrounding a heptane/water droplet. The results show that increasing the amount of water in the emulsion decreases the peak (flame) temperature as illustrated for 70% and 90% by volume heptane/water emulsion droplets (with $r_d = 0.30$ mm). While the present model predicts a peak temperature of approximately 2060 K for a pure heptane flame, 30% water addition lowers the peak gas temperature to about 1880 K. Concerning the OH profiles, they rise much more rapidly with increased water content due to smaller flames, but they also have sharper peaks as well.

Both the peak gas temperature decreases and the peak OH concentration moves inward (either one of which is sometimes taken as the flame position) as the water content in the liquid phase is increased as shown in Figure 10. The former point is further illustrated in Figure 11 which shows the variation of peak gas temperature, and location of that peak (r_f/r_d), with increasing water

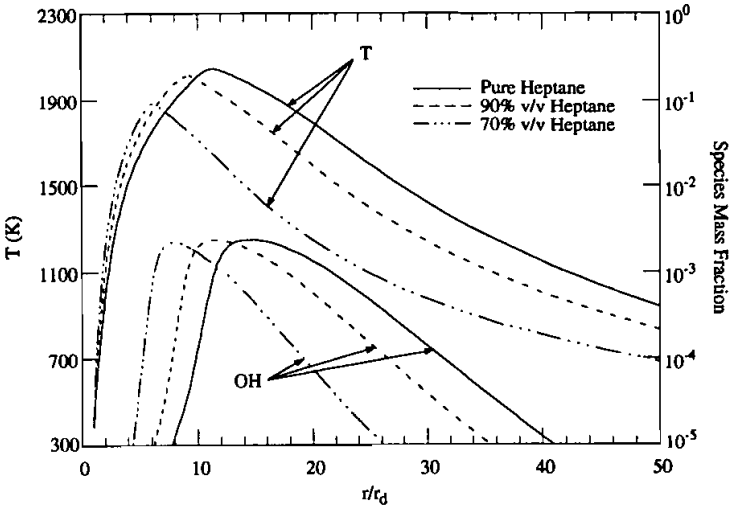

FIGURE 10 Variation of gas phase temperature and OH species with radial location around a heptane/water mixture droplet.

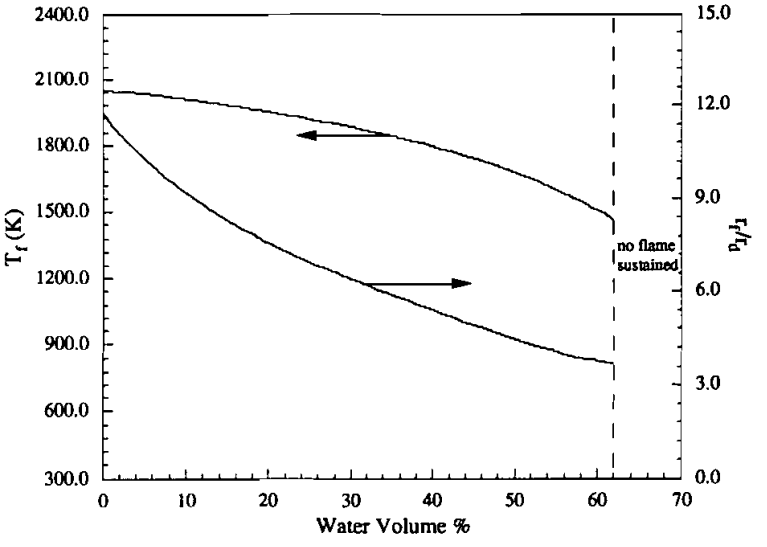

FIGURE 11 Variation of flame temperature and flame radius with water volume percent for a 0.3 mm radius droplet.

content. The decrease in the flame diameter with increasing water content may arise from the increase in the heat of vaporization of the mixture as water is added to the fuel. While heptane has a heat of vaporization of 317 J/g, the heat of vaporization for water is 2263 J/g. The increased heat of vaporization due to the water requires steeper gas phase temperature gradients at the droplet surface to maintain vaporization rates to sustain combustion. Thus, the flame moves closer to the droplet surface as shown in Figure 11. For high enough water content, the required temperature gradients become too steep for the heat release provided by the fuel and stable burning stops.

Figure 11 shows that both the flame temperature and the flame diameter are reduced as the water content is increased. The reduction in the flame diameter as well as the decrease in temperatures inside the flame where fuel pyrolysis occurs should cause the propensity for soot formation to decrease with increasing liquid water content. Figure 12 illustrates the variation of $\dot{m}_{soot}$, calculated from eq. 11, with water content for $r_d = 0.3$ mm. The results show that soot formation for a given amount of fuel falls off quite rapidly as the water content is increased and in fact is reduced by 3 orders of magnitude for 50% by voume water addition.

Burning rates for heptane/water mixture droplets were calculated to decrease as liquid water content increased. Figure 13 shows this trend (solid line)

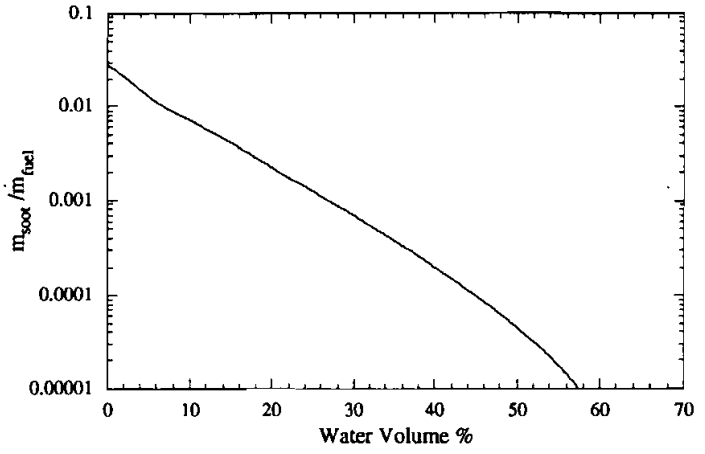

FIGURE 12 Effect of water concentration on fractional conversion of vaporized heptane to soot.

for $r_d = 0.3$ mm. Stable burning existed up to about 60% water volume percent for $r_d = 0.3$ mm, after which, according to Figure 13, the flame temperature evidently dropped to a low enough value that burning could not be sustained. Results are also compared to a quasi-steady, constant property model for spherically symmetric emulsion droplet combustion. The burning rate from the constant property model according to the classical theory (e.g., Glassman 1987) is calculated from

$$K = \frac{8\lambda}{\rho_1 C_p} \ln(1 + B) \tag{12}$$

where $\rho_1 = \phi\rho_w + (1-\phi)\rho_f$, $C_p = \phi C_{pw} + (1-\phi)C_{pf}$ and $\lambda = k_g x + (1-x)k_f$. It has been shown (Law, 1977) that for 'frozen', quasisteady, and constant property spherically symmetric combustion of an emulsion droplet experiencing a single step reaction process

$$B = \frac{Q_f Y_{0\infty}}{v_0 L_f}\left[\frac{1 + \dfrac{C_p(T_\infty - T_s)}{Q_f Y_{0\infty}/v_0}}{1 + \varepsilon_w \dfrac{L_w}{L_f}\left(1 - \dfrac{L_f}{L_w}\right)}\right] \tag{13}$$

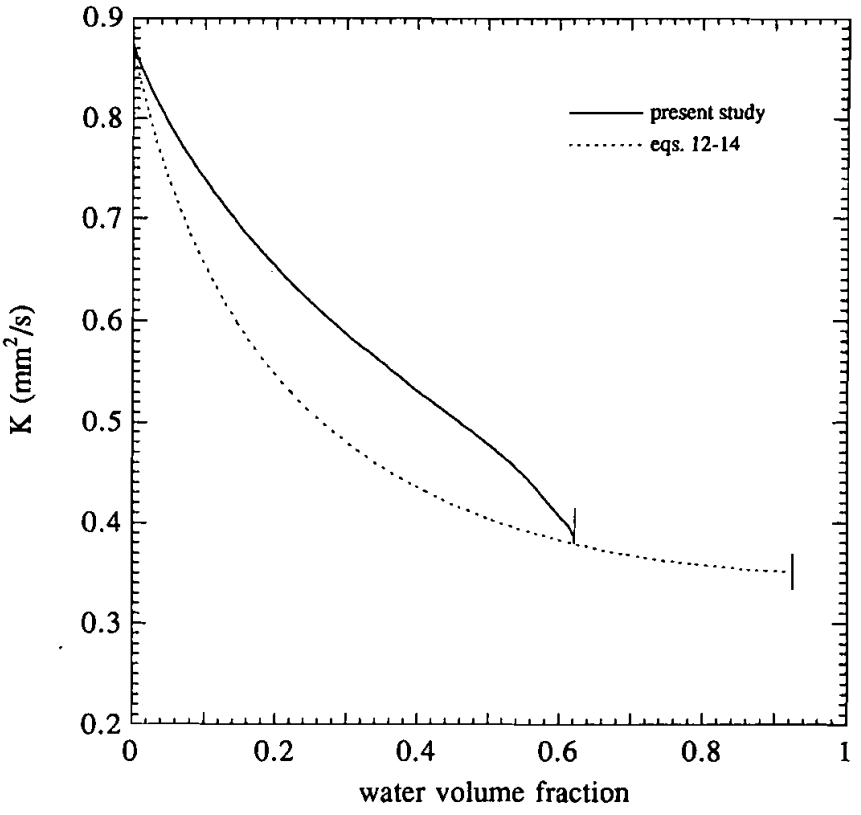

FIGURE 13 Droplet burning rate from present model compared with a constant property, single step reaction model.

ε_w is related to the water volume fraction, ϕ, as

$$\phi = \frac{1}{\frac{\rho_w}{\rho_f}\left[\frac{1-\varepsilon_w}{\varepsilon_w}\right]+1} \tag{14}$$

Because the analysis which led to eq. 13 assumes constant properties, and the selection of the property values strongly effects gasification rate predictions, for purposes of comparison we chose property values in eqs. 12–14so that the predicted gasification rate would match that of pure heptane ($\phi = 0$) calculated from the present study. For this purpose, x was simply adjusted to 0.7 to achieve the match. The other properties are evaluated at a mean tempera-

TABLE II Property Values for Eqs. 12–14

C_{pf}(1338 °K)	1.024 cal/gm – K
C_{pw}^{pp}(1338 °K)	.599
ρ_f(372 °K)	.614 g/cm^3
ρ_w(372 °K)	.958 g/cm^3
k_g(1338 °K)	1.94×10^{-4} cal/cm-s-K
k_f(1338 °K)	3.39×10^{-4} cal/cm-s-K
v_0	11
$Y_{0\infty}$	.232
Q_f	11,607 cal/gm
T_∞	300 K
T_s	372 K
L_f(372 °K)	75.6 cal/gm
L_w(372 °K)	539.36 cal/gm

ture between the droplet and flame, as listed in Table 1and were taken from Touloukian *et al.*, (1970) and Vargaftik (1975).

There are substantial differences between eqs. 12–14(dotted line) and the present calculation as shown in Figure 13. The assumptions concerning property values (variable versus constant) and combustion chemistry (single step versus complex) cause the differences shown. The limit of stable burning predicted from the single step, constant property formulation (indicated by the vertical bar at end of curves in Figure 13, occurs at a higher water content and corresponds to a well defined (mathematical) limit of $r_f/r_d = 1$. When the present complex chemistry model is used, stable flames are calculated down to only 38% by volume heptane. Below this liquid concentration of heptane the flame temperature drops below a point at which combustion can no longer sustain droplet vaporization and fuel pyrolysis. As indicated in Figure 11, this is realized well before $r_f = r_d$.

6. SUMMARY

When complex chemistry is considered in a droplet flame model, predicted C_2H_2 species profiles produced during combustion of heptane/water mixture droplets vary with droplet size and water content. The predicted burning rates are higher than experimental values and independent of droplet size, which can be attributed to the inability of the model to account for the lowering of the heat release at the flame due to soot formation. However, fractions of vaporized fuel leading to soot formation were shown to decrease with decreas-

ing droplet size due to smaller flames and less time for fuel pyrolysis. Also, the addition of water to heptane is also shown to decrease flame diameters and thereby reduce significantly the time for fuel pyrolysis and hence soot formation. Burning rate constants and flame temperatures both decrease as water content increases.

The present model has limits in that it does not account for the transient development of concentration gradients inside the droplet and of the gas phase species profiles. Transient effects in the liquid phase are significant for multicomponent fuels, and the gas phase transient effects are important for all fuels early and late in the burning process. To incorporate these effects, the liquid phase must be modeled for droplet heating and changes in fuel composition with time. Nonetheless, the model in its current from does provide information on trends that aid in our understanding of the structure of droplet flames for fuels which do not significantly alter their liquid composition during combustion.

Acknowledgements

The authors acknowledge the financial support of the National Aeronautics and Space Administration and the New York State Center for Hazardous Waste Management (Dr. A. Scott Weber, project monitor). GSJ received further support from the NASA Graduate Student Researchers Program. The authors also wish to thank Professor Merwin Sibulkin of Brown University for reading the manuscript and offering constructive comments. CTA also wishes to thank Professor Richard Dobbins of Brown University for his hospitality during preparation of the manuscript.

References

Bui-Pham, M. and Seshadri, K. (1991). Comparison between Experimental Measurements and Numerical Calculations of the Structure of Heptane-Air Diffusion Flames. *Comb. Sci. Tech.*, **79**, 293.

Card, J. M. and Williams, F. A. (1991). Asymptotic Analysis of Spherically Symmetrical n-Heptane Diffusion Flames with Variable Properties. *Comb. Flame*, **91**, 187.

Chauveau, C., Chesneau, X. and Gökalp, I. (1993). Burning Characteristics of *n*-Heptane Droplets under Different Regimes. *AIAA* Paper No. 93-0824.

Cho, S. Y., Choi, M. Y., and Dryer, F. L. (1991). Extinction of a Free Methanol Droplet in Microgravity. *23rd Symposium (International) on Combustion.*, pp. 1611.

Cho, S. Y., Yetter, P. A., and Dryer, F. L. (1992). Computer Model for Chemically Reactive Flow with Complex Chemistry/Multicomponent Molecular Diffusion/Heterogeneous Processes. *J. Comp. Phys.*, **102**, 160.

Choi, M. Y., Dryer, F. L., and Haggard, J. B. (1990). Observations of a Slow Burning Regime for Hydrocarbon Droplets. *23rd Symposium (International) on Combustion.*, Pittsburgh, Pa.: The Combustion Institute, pp. 1597.

Coffee, T. P. and Heimerl, J. M. (1981). Transport Algorithms for Premixed Laminar Steady State Flames. *Comb. Flame*, **43**, 273.

Fairweather, M., Jones, W. P. and Lindstedt, R. P. (1992). Predictions of Radiative Transfer from a Turbulent Reacting Jet in a Cross-Wind. *Comb. Flame*, **89**, 45.

Glassman, I. (1987). *Combustion*, 2nd ed., Orlando, Fla.: Harcourt, Brace, Jovanovich.

Glassman, I. (1988). Soot Formation in Combustion Processes. *22nd Symposium (International) on Combustion.*, Pittsburgh, Pa.: The Combustion Institute, pp. 295.

Gupta, S. B., Ni, T., and Santoro, R. J. (1994). Spatial and Time-Resolved Soot Volume Fraction Measurements in Methanol/Benzene Droplet Flames. presented at the Fall Eastern States Section Meeting, Combustion Institute, paper no. 50, Clearwater Beach, Fl., December 5.

Haynes, B. S. and Wagner, H. (1981). Soot Formation. *Prog. Energy Comb. Sci.*, **7**, 229.

Jackson, G. S. and Avedisian C. T. (1994). The Effect of Initial Droplet Diameter in Spherically Symmetric Droplet Combustion of Sooting Fuels. *Proc. R. Soc. Lond.*, A**446**, 255.

Jackson, G. S., Avedisian, C. T. and Yang, J. C. (1992). Observations of Soot during Droplet Combustion at Low Gravity: Heptane and Heptane/Monochloroalkane Mixtures. *Int. J. Heat Mass Trans.*, **35**(8), 2017.

Jackson, G. S. (1994). Spherically Symmetric Droplet Combustion of Sooting and Multicomponent Fuels. Ph.D. Thesis, Cornell University, Ithaca, NY.

Kee, R. J., Dixon-Lewis, G., Warnatz, J., Coltrin, M. E., and Miller, J. A. (1986). A FORTRAN Computer-Code Package for the Evaluation of Gas-Phase Multicomponent Transport Properties. Sandia National Laboratories Report, SAND86-8246.

Kee, R. J., Rupley, F. M., and Miller, J. A. (1987). The CHEMKIN Thermodynamic Database. Sandia National Laboratories Report, SAND87–8215B.

Kesten, A. S., Sangiovanni, J. J., and Goldberg, P. (1980). Conceptual Examination of Gas Phase Particulate Formation in Gas Turbine Combustors. *J. Eng. for Power*, **102**. 613.

Law, C. K. (1977). A Model for the Combustion of Oil/Water Emulsion Droplets. *Comb. Sci. Tech.* **17**, 29.

Linstedt, R. P. and Maurice, L. Q. (1995). Detailed Kinetic Modeling of *n*-Heptane Combustion, *Comb. Sci. Tech.*, **107**, 317.

Okajima, S. and Kumagai, S. (1975). Further Investigations of Combustion of Free Droplets in a Freely Falling Chamber Including Moving Droplets. *15th Symposium (International) on Combustion.*, p. 401.

Puri, I. and Libby, P. A. (1991). The Influence of Transport Properties on Droplet Burning. *Comb. Sci. Tech.*, **76**, 67.

Saitoh, T., Yamazaki, K. and Viskanta, R. (1993). Effect of Thermal Radiation on Transient Combustion of a Fuel Droplet, *J. Thermophys. Heat Transf.*, **7**, 94.

Smooke, M. D. (1991). "Numerical Modeling of Laminar Diffusion Flames", in *Numerical Approaches to Combustion Modeling, Prog. in Astronautics and Aeronautics* (E. S. Oran and J. P. Boris Eds.), *AIAA*, **135**, Ch. 7.

Talbot, L., Cheng, R. K., Schefer, R. W., and Willis, D. R. (1980). Thermophoresis of Particles in a Heated Boundary Layer. *J. Fluid Mechanics*, **101**, 737.

Touloukian, Y. S., Liley, P. E. and Saxena, S. C. (1970). *Thermophysical Properties of Matter*, vol. 3., Plenum, New York.

Vargaftik, N. B. (1975). *Handbook of Physical Properties of Liquids and Gases*, 2nd ed., Hemisphere Publishihing Co., New York.

Wang, C. H. (1983). Combustion and Micro-explosion of Multicomponent Droplets. Ph.D. Thesis Northwestern University.

Warnatz, J. (1984). Chemistry of High Temperature Combustion of Alkanes up to Octane. *20th Symposium (International) on Combustion*, p. 845.

Westbrook, C. K. (1986). Chemical Kinetic Modeling of Higher Hydrocarbon Fuels. *AIAA J.*, **24**, 2002.

Williams, F. A. (1985). *Combustion Theory*, 2nd. ed., Benjamin/Cummings, Menlo Park, CA.